Optics Letters

Optofluidic biomolecule sensors based on a-Si:H microrings embedded in silicon–glass microchannels

T. Lipka,* L. Moldenhauer, L. Wahn, and H. K. Trieu

Institute of Microsystems Technology, Hamburg University of Technology, Eissendorferstr. 42, Hamburg, Germany
**Corresponding author: timo.lipka@tuhh.de*

Received 24 January 2017; revised 10 February 2017; accepted 10 February 2017; posted 14 February 2017 (Doc. ID 285523); published 6 March 2017

The large-scale and low-cost fabrication of high sensitivity sensors for the real-time detection of biochemicals and molecular substances opens up new opportunities in the areas of bioanalytic screening and medical diagnostics. Planar integrated photonic resonators that can be fabricated with a low footprint, in spatial and wavelength multiplexed arrangements, and that enable integration with microfluidics on the wafer scale have emerged as a promising sensing platform for these application fields. We realized an optofluidic and label-free biosensor that is based on hydrogenated amorphous silicon microring resonators embedded in silicon/glass microfluidic channels for analyte injection and biomolecule immobilization. The optofluidic sensor merits for refractive index and biomolecule sensing are evaluated by sensitivity and detection limit simulations, whereas a proof of concept is demonstrated by real-time protein immobilization experiments of functionalized resonators.

OCIS codes: (170.0170) Medical optics and biotechnology; (220.4241) Nanostructure fabrication; (250.5300) Photonic integrated circuits; (280.1415) Biological sensing and sensors.

https://doi.org/10.1364/OL.42.001084

Photonic microcavities are promising sensors to measure biochemical substances and to monitor biomolecule binding events and kinetics on microscale areas with high sensitivities (S) and low detection limits (LoD), down to single molecules [1]. Since the early proposals and demonstrations of molecule detection with optical microcavities [2,3], significant progress has been reported within the diverse fields of biomolecular layer sensing (BMLS) and refractive index sensing (RIS) by employing various optical materials, sensor devices, and analyte species [4,5]. While high-quality microspheres due to their narrow resonance linewidth provide new prospects for ultra-low detection limits with fast interrogation methods, the superior quality of integrated photonics results from the wafer-scale manufacturing and the possibility to construct biosensor arrays of high complexity with minimal footprint. Hence, a variety of planar integrated optical sensors such as microring resonators (MRRs) [6], Mach–Zehnder-interferometers [5], and optimized structures (e.g., photonic crystal [7], slotted [8], and sub-wavelengths grating waveguides [9]) have been reported.

In this Letter, we present a versatile optofluidic sensor platform for BMLS and RIS that is manufactured with amorphous silicon (a-Si:H) photonic MRRs and microfluidic channels based on silicon/glass process technology, respectively, thus enabling low-cost and high-throughput fabrication. The optofluidic sensors are schematically illustrated in Fig. 1. Favorable properties of the sensor platform result from the flexible a-Si:H process, which allows depositing high refractive index layers on various substrates with arbitrary layer thickness [10], and with high uniformity on wafer-scale [11]. The employment of robust silicon/glass for the microfluidics provides advantageous properties compared to polymers in terms of high chemical inertness, dimensional stability, negligible permeability, low affinity to adsorption of small molecules, and long-term stability. Compared to analytic biochemistry based on microwell plates, e.g., enzyme linked immunosorbent assays (ELISA), silicon photonic sensors allow minimization of such test kit sizes by 2–3 orders of magnitude (12.7 cm × 8.5 cm [12] versus, e.g., 5 mm × 5 mm) with a similar number of sensors and a label-free quantification method, while providing the potential for comparable detection performance [13,14].

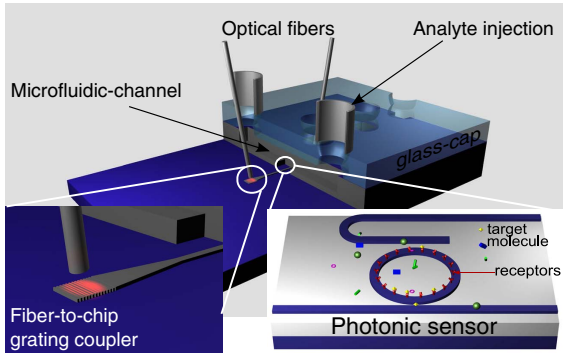

Fig. 1. Illustration of the biosensor based on photonic microresonators embedded in silicon/glass fluidic channels.

In particular, high refractive index MRRs are very attractive for BMLS applications because the multiple light roundtrips within the cavity provide distinct and sharp resonance peaks for small physical device lengths [15]. The small ring surface facilitates low LoD and the large free spectral range (FSR) provides excellent opportunities to realize spatial and wavelength multiplexed arrays for the simultaneous interrogation of multiple sensors [6,16–18]. The sensing concept is based on the light interaction via the evanescent field of the resonant mode with the analyte medium and/or the adsorpted molecules at the MRR surface. The fundamental guided modes (TE, TM) of the photonic waveguides were determined by a finite element method mode solver (COMSOL). The sensors were modeled by the well-known MRR equations [19]. The resonance condition is satisfied for multiple equals of 2π with the round-trip phase $\phi = \beta L_r = 2\pi n_{\text{eff}} L_r \lambda^{-1}$ related to the propagation constant β by the guided optical mode n_{eff} for a MRR length L_r. If the analyte varies in the refractive index, this change is transduced into a wavelength shift $\Delta\lambda_r$, which is linearly proportional to the analyte quantity and can be measured with very high accuracy at resonance, $\lambda_r \cdot m = L_r \cdot n_{\text{eff}}$, with m as guided mode order. The key metrics of the optofluidic sensor are the sensitivity and the detection limit. The sensitivity (S_{RIU}) of the MRR in terms of refractive index units is defined as

$$S_{\text{RIU}} = \frac{\Delta\lambda_r}{\Delta n_a} = \frac{\lambda_r}{n_g}\frac{\partial n_{\text{eff}}}{\partial n_a}, \tag{1}$$

with the analyte index n_a and group index $n_{gr} = n_{\text{eff}} - \lambda\frac{dn_{\text{eff}}}{d\lambda}$, accounting for chromatic dispersion. Instead, the sensitivity for the detection of molecules is conventionally described by the adsorption of a molecular layer with thickness t_{ml}:

$$S_{\text{ml}} = \frac{\Delta\lambda_r}{\Delta t_{\text{ml}}} = \frac{\lambda_r}{n_g}\frac{\partial n_{\text{eff}}}{\partial t_{\text{ml}}}\bigg|_{n_{\text{ml}}}, \tag{2}$$

which is related to n_{ml}, the equivalent refractive index of the adsorpted BML [20]. Although refractive index, thickness, and thin film density differentiations are rather complex due to the preferential sticking orientation of the molecules forming the biomolecular layers, this approach has been widely applied to model the adsorption to integrated-optic sensors; experimental verifications have been presented by several research works, e.g., [21,22], which in addition provide methods on how to retrieve the refractive index and layer thickness simultaneously.

The optofluidic sensor response at $\lambda = 1.55$ μm for different molecular layer thicknesses is shown in Fig. 2. The a-Si:H and SiO_2 indices of $n = 3.48$ and $n = 1.456$ were measured by ellipsometry [23], the water index was implemented as $n = 1.32$, and the BML was modeled with a density of $\rho = 1.33\ \text{g cm}^{-3}$ and $n_{\text{ml}} = 1.45$. According to this, the RIS sensitivities of $S_{\text{RIU,TE}}$=66nm/RIU and $S_{\text{RIU,TM}}$=243nm/RIU were determined for the photonic wire waveguides of 480 × 200 nm dimension, whereas for BMLS up to 10 nm thickness, $S_{\text{ml,TE}} = 155$ pm/nm and $S_{\text{ml,TM}} = 263$ pm/nm were identified. In both cases the sensitivity can be further enhanced by maximizing the mode confinement within the analyte medium or the molecular layer using a target application-optimized waveguide geometry. The detection limits for BMLS and RIS were determined according to Eqs. (3) and (4) [24]. In the following, the theoretical LoD is analyzed for an absolute readout resolution; further important influencing factors such as the peak extinction ratio and linewidths, thermal fluctuations,

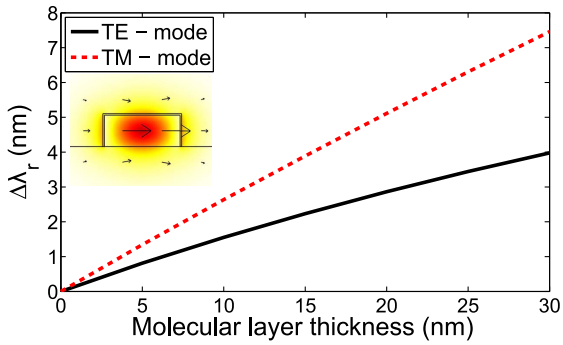

Fig. 2. Optofluidic sensor response for both guided modes due to a molecular thin film adsorpted on the photonic resonator surface. A simulation of the TE guided mode is inset.

system noise, and the light source spectral bandwidth on the sensor performance have been evaluated in more detail in [25,26]. The relevant m-orders for the LoD analysis were numerically calculated by the n_{eff} crossings as shown in Fig. 3. The minimal detectable analyte index can be determined from

$$\text{LoD}_n = \frac{m}{L_r}\left(\frac{\partial n_{\text{eff}}}{\partial n_a}\right)^{-1}\Delta\lambda_{r,\text{min}}, \tag{3}$$

whereas the adsorbed biomolecule mass is approximated by

$$\text{LoD}_M = A\rho\frac{m}{L_r}\left(\frac{\partial n_{\text{eff}}}{\partial t_{\text{ml}}}\right)^{-1}\Delta\lambda_{r,\text{min}}. \tag{4}$$

The theoretical results are summarized in Fig. 4 and provide LoD_n of $8.2 \cdot 10^{-6}$ and $2.3 \cdot 10^{-6}$ for the TE and TM modes, respectively, and a LoD_M varying between 565 and 70 ag for TE depending on the MRR surface A at a readout resolution of $\Delta\lambda_{r,\text{min}} = 1$ pm; due to the lower TM mode confinement ($\Gamma_{\text{TM}} \approx 0.25$ versus $\Gamma_{\text{TE}} \approx 0.75$), only TE is considered. Since the $\frac{m}{L_r}$ ratio is widely independent of the MRR lengths down to very short perimeters where mode de-confinement occurs, LoD_n is merely defined by the modal sensitivity due to $\frac{\partial n_{\text{eff}}}{\partial n_a}$ and $\lambda_{r,\text{min}}$. As a consequence, MRR-based refractometers perform better for larger ring radii because weakly guided modes with strong analyte interaction provide higher Q-factors. Compared to this, LoD_M scales with the surface area, whereas $\Delta\lambda_r$ is independent of MRR size, and hence, the same surface coverage yields distinctly lower detection limits using ultracompact MRRs, e.g., with 3–4 μm in diameter. This important

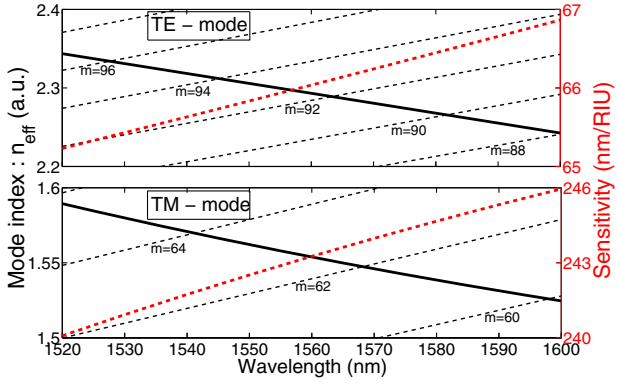

Fig. 3. Effective mode index, resonance order, and sensitivity of a 10 μm radius microring resonator for TE and TM.

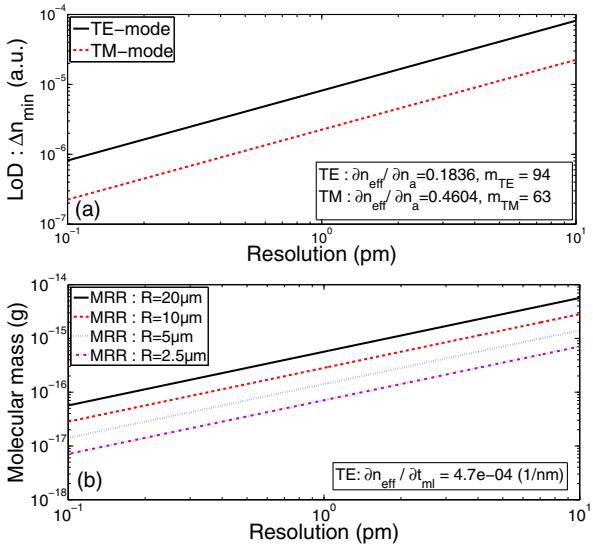

Fig. 4. Limit-of-detection calculations against wavelength resolution: (a) Refractive index sensing. (b) Biomolecule surface sensing.

physical attribute and the strong evanescent field at the low/high refractive index interfaces improve the potential LoD_M significantly. Although the reduced resonance linewidth opposes the potential resolution with conventional wavelengths scanning methods, interrogation concepts, e.g., based on frequency locking [27], cavity ring down [28], or fast Fourier transform techniques [29], promise low LoD despite the aforementioned detriments.

A schematic representation of the optofluidic biosensor manufacturing sequence is provided in Fig. 5. The fabrication basically consists of three fabrication steps: (1) the photonic systems were manufactured on silicon wafers (10 cm diameter), 3 μm bottom oxide cladding layer, and with 200 nm a-Si:H as the guiding core layer deposited by plasma enhanced chemical vapor deposition. The fiber-to-chip couplers, photonic wires, and resonators were patterned with electron beam lithography and structured by an anisotropic dry etch process with a continuous C_4F_8/SF_6 flow in an inductively coupled plasma. (2) The fluidic microchannels were fabricated in a chemically stable silicon/glass (boron silicate) stack. For that, a dual-side polished (DSP) silicon wafer of 500 μm thickness was covered with a glass wafer that enclosed the channels and allowed injecting the analyte through the inlet tubes and coupling light to the photonic sensors. In the first step, the silicon wafer was structured on both sides by two g-line photo-lithography and etch steps. The fluidic microchannels for the analyte transport were defined on one side and the wafer was anisotropically etched by deep reactive ion etching to a depth of approximately 150 μm. Subsequently, the opposite side was patterned and the photonic sensing windows and the optical fiber vias were etched through the wafer. After that, the upper glass sealing was covered with a polysilicon layer, deposited by low pressure chemical vapor deposition, which served as a hard mask and was photo-patterned and structured from both sides with wet chemical etching using hydrofluorid acid (49%), followed by removing the hard mask in potassium hydroxide (KOH). The silicon and glass substrates were anodically bonded at 300°C such that an irreversible and robust bond that resists high fluidic pressures was formed. (3) The photonic and the microfluidic chips were aligned and bonded by using a fineplacer. Finally, the inlet tubes for the fluidic channels were glued to the biosensor.

As a proof of concept to measure specific biomolecules, e.g., DNA, proteins, bacteria, and viruses, etc., binding to the resonator cavity, the a-Si:H sensor chip was functionalized. The chip surface was cleaned and pre-activated with an amine-reactive homobifunctional-crosslink in order to allow the label-free sensing of bovine serum albumin (BSA). The 10 μm radius add/drop MRR with loaded Q-factors of about $0.7 \cdot 10^4$ operates near critical coupling and provides 25 dB drop port extinction with the aqueous top cladding of deionized water (DIW), which is beneficial for high sensitivities and low detection limits. The microring sensors were characterized in immobilization experiments with optical transmission measurements. Single-mode fibers with 10 μm mode-field-diameter were inserted through the optical vias of the Si/glass sealing and aligned to polarization selective (TE) grating couplers [15]. The BSA proteins were dissolved in DIW and injected by a pressure-driven flow syringe pump (AL-1000, WPI). Five concentrations (0.1, 0.5, 1, 10, 100 μg/mL), which were stored at the same ambient temperature prior to use, were successively supplied by the microfluidic channels while monitoring the optical spectra. Therefore, the tunable laser source (Agilent 8164B) was continuously scanned from 1530 to 1570 nm with −4.5 dBm input power and the transmitted intensity was data-logged with 10 pm resolution, while the sensors were temperature-stabilized to $T_{\mathrm{rms}} \approx 5$ mK by the chip mount (equals $\Delta\lambda_{r,\mathrm{rms}} \approx 0.4$ pm).

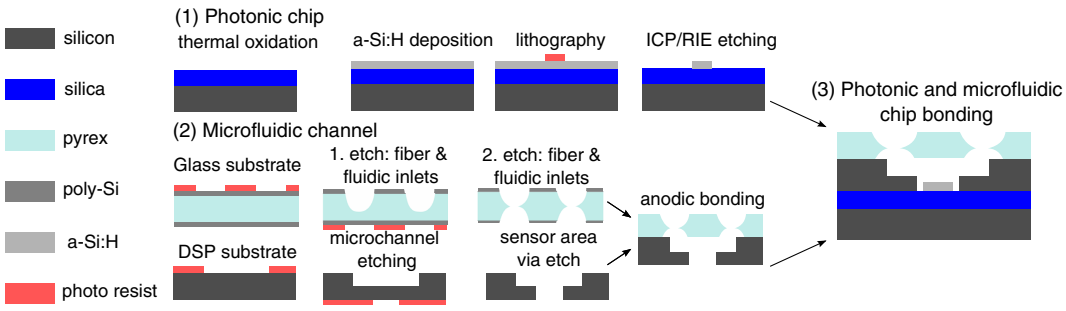

Fig. 5. Optofluidic chip fabrication based on two silicon and one glass wafer (not to scale): 1. the photonic systems with the fiber-chip-couplers, waveguides, and biosensing resonators are manufactured. 2. The microfluidic channels are fabricated in a robust silicon/glass stack to supply the sensors with the analyte. 3. The photonic and microfluidic parts are merged.

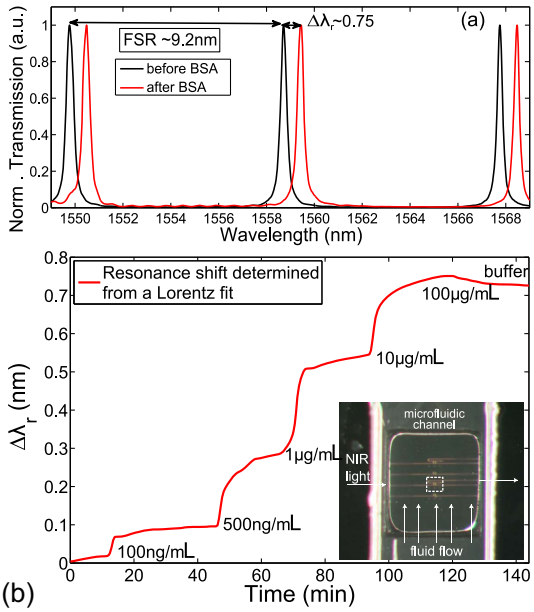

Fig. 6. (a) Microring drop port spectra before and after BSA. (b) Measurements for increasing BSA concentrations over time; a top-view micrograph captured through the glass cap is inset.

For the analysis, the drop port resonance peak maxima were extracted by using a Lorentz fit. The results of the protein immobilization are given in Fig. 6, where the wavelength shift kinetics for the different BSA concentrations are plotted over time. The overall shift after flowing the sensor subsequently for about 20 min with pure DIW accounts for $\Delta\lambda_r \approx 0.72$ nm. This corresponds to a uniform BML thickness of $t_{\mathrm{ml}} \approx 4$–$5$ nm (Fig. 2) or a surface coverage of 55%–60%, which is in good agreement with our preliminary studies [30], and in accordance with the 14 nm × 4 nm × 4 nm BSA protein size [31]. However, because refractive index and thickness changes are influenced by how the molecules adsorb on the sensor surface (e.g., side-on or end-on orientation), reference rings with different sensitivities or polarizations need to be employed to detect reliable data for both metrics in one measurement cycle, which is worthwhile for prospective research. In addition, note that this proof of concept measurement was not intended to determine the best possible resolution and that the peripheral components to access the optofluidic sensor with flexible silicone tubes were not optimized. In order to evaluate the sensor performance in terms of LoD, we conducted repetitive measurements with 1 pm scans under ideal conditions, and deviations of $\Delta\lambda_{r,\mathrm{rms}} \approx 0.3$ pm were achieved over 90 minutes. Hence, with an adequate off-chip temperature control or an on-chip reference, the sensors provide the potential to measure refractive index changes down to $\mathrm{LoD}_n \approx 10^{-6}$ and biomolecules with $\mathrm{LoD}_M \approx 10^{-16}$ g, predominantly enhanced by small microring surface areas.

In conclusion, an optofluidic sensor for the label-free detection of biomolecules and for RIS is presented. The modular manufacturing facilitates the fabrication of wafer-scale photonic sensors and microfluidic systems for the analyte transport using well-established technologies. The label-free detection is demonstrated with real-time BSA protein immobilization experiments. The low-cost manufacturing and the versatile processing options promise capabilities to develop lab-on-chip sensors for various kinds of analyte species relevant for chemical and bioanalytic sensing applications.

REFERENCES

1. J. Su, A. F. Goldberg, and B. M. Stoltz, Light Sci. Appl. **5**, e16001 (2016).
2. R. W. Boyd and J. E. Heebner, Appl. Opt. **40**, 5742 (2001).
3. F. Vollmer, D. Braun, A. Libchaber, M. Khoshsima, I. Teraoka, and S. Arnold, Appl. Phys. Lett. **80**, 4057 (2002).
4. M. S. Luchansky and R. C. Bailey, Anal. Chem. **84**, 793 (2012).
5. M. Estevez, M. Alvarez, and L. Lechuga, Laser Photon. Rev. **6**, 463 (2012).
6. M. Iqbal, M. A. Gleeson, B. Spaugh, F. Tybor, W. G. Gunn, M. Hochberg, T. Baehr-Jones, R. C. Bailey, and L. C. Gunn, IEEE J. Sel. Top. Quantum Electron. **16**, 654 (2010).
7. N. Skivesen, A. Tetu, M. Kristensen, J. Kjems, L. H. Frandsen, and P. I. Borel, Opt. Express **15**, 3169 (2007).
8. F. Dellâ Olio and V. M. N. Passaro, Opt. Express **15**, 4977 (2007).
9. J. Flueckiger, S. Schmidt, V. Donzella, A. Sherwali, D. M. Ratner, L. Chrostowski, and K. C. Cheung, Opt. Express **24**, 15672 (2016).
10. T. Lipka, O. Horn, J. Amthor, and J. Müller, J. Eur. Opt. Soc. **7**, 12033 (2012).
11. T. Lipka, J. Müller, and H. K. Trieu, J. Lightwave Technol. **34**, 3163 (2016).
12. https://www.slas.org/resources/information/industry-standards (accessed 10 February 2017).
13. L. Chrostowski, S. Grist, J. Flueckiger, W. Shi, X. Wang, E. Ouellet, H. Yun, M. Webb, B. Nie, Z. Liang, K. C. Cheung, S. A. Schmidt, D. M. Ratner, and N. A. F. Jaeger, Proc. SPIE **8236**, 823620 (2012).
14. J. T. Kindt, M. S. Luchansky, A. J. Qavi, S.-H. Lee, and R. C. Bailey, Anal. Chem. **85**, 10653 (2013).
15. T. Lipka, L. Moldenhauer, J. Müller, and H. K. Trieu, Photon. Res. **4**, 126 (2016).
16. D.-X. Xu, M. Vachon, A. Densmore, R. Ma, A. Delâge, S. Janz, J. Lapointe, Y. Li, G. Lopinski, D. Zhang, Q. Y. Liu, P. Cheben, and J. H. Schmid, Opt. Lett. **35**, 2771 (2010).
17. T. Lipka, L. Moldenhauer, J. Muller, and H. Trieu, IEEE Photon. J. **7**, 1 (2015).
18. J. H. Wade, A. T. Alsop, N. R. Vertin, H. Yang, M. D. Johnson, and R. C. Bailey, ACS Cent. Sci. **1**, 374 (2015).
19. A. Yariv, Electron. Lett. **36**, 321 (2000).
20. J. Vörös, Biophys. J. **87**, 553 (2004).
21. Y. Atsumi, D.-X. Xu, A. Delâge, J. H. Schmid, M. Vachon, P. Cheben, S. Janz, N. Nishiyama, and S. Arai, Opt. Express **20**, 26969 (2012).
22. J.-W. Hoste, S. Werquin, T. Claes, and P. Bienstman, Opt. Express **22**, 2807 (2014).
23. T. Lipka, L. Moldenhauer, J. Müller, and H. K. Trieu, Opt. Express **23**, 20075 (2015).
24. K. D. Vos, I. Bartolozzi, E. Schacht, P. Bienstman, and R. Baets, Opt. Express **15**, 7610 (2007).
25. J. Hu, X. Sun, A. Agarwal, and L. C. Kimerling, J. Opt. Soc. Am. B **26**, 1032 (2009).
26. F. Ghasemi, H. Zhou, and A. Adibi, IEEE J. Sel. Top. Quantum Electron. **21**, 419 (2015).
27. L. Stern, I. Goykhman, B. Desiatov, and U. Levy, Opt. Lett. **37**, 1313 (2012).
28. M. I. Cheema, S. Mehrabani, A. A. Hayat, Y.-A. Peter, A. M. Armani, and A. G. Kirk, Opt. Express **20**, 9090 (2012).
29. L. Gounaridis, P. Groumas, E. Schreuder, R. Heideman, H. Avramopoulos, and C. Kouloumentas, Opt. Express **24**, 7611 (2016).
30. T. Lipka, L. Wahn, H. K. Trieu, L. Hilterhaus, and J. Müller, J. Nanophoton. **7**, 073793 (2013).
31. A. Wright and M. Thompson, Biophys. J. **15**, 137 (1975).